

Modeling of the coupled dynamics of damping particles filled in the cells of a honeycomb sandwich plate and experimental validation

Nazeer Ahmad[#], R. Ranganath[#], Ashitava Ghosal^{§*}

[#] ISRO Satellite Centre,
Indian Space Research Organization,
Vimanapura Post, Bangalore 560017, India
nazeer@isac.gov.in, rrrr@isac.gov.in

[§] Department of Mechanical Engineering
Indian Institute of Science, Bangalore 560012, India
asitava@iisc.ac.in

* Corresponding author

Abstract

Equipment panels of a spacecraft are made up of a sandwich composite with aluminium face sheets and a honeycomb (HC) core. The honeycomb sandwich plate responds to the launch vibration loads subjecting the equipment mounted on it to a high level of accelerations at resonances owing to a lower natural damping. Damping particles (DPs) when inserted in the empty cells of a HC core improve the damping characteristics and reduce the resonance responses. In this work, we present a mathematical model governing the motion of the cell walls, DPs and HC plate under dynamic loading. Discrete element method (DEM) has been used to model the dynamics of the DPs wherein the contacts are modeled using modified nonlinear dissipative Hertz contact theory in conjunction with Coulomb friction. The effect of DPs on the responses at resonances, damping and frequency response function (FRF) of the HC plate is obtained. Numerical and experimental studies were conducted on a HC plate where a selected portion of the plate was filled with DPs. The HC plate was subjected to sine sweep base acceleration at the edges to study the effect of DPs on the dynamic characteristic of the plate. The damping ratios and resonance peaks of the lower

four modes of the HC plate, excited up to 1000 Hz, obtained experimentally from the FRF measurements and numerically from the DEM model compare well. The damping ratios, response at resonances and the FRF profiles are also similar. Significant improvement in damping ratios and attenuation of vibration level has been observed.

Keywords

Spacecraft structures, particle impact damping, honeycomb sandwich plate, discrete element method, and passive vibration control

Nomenclature

L, W, t	length, width and thickness of the plate
t_c	thickness of the honeycomb core
$\mathbf{M}, \mathbf{C}, \mathbf{K}$	mass, damping and stiffness matrices
$\mathbf{f}^d, \mathbf{f}^e$	impact damping and external excitation force vector
$\boldsymbol{\chi}$	generalized displacement vector
R	radius of the circle circumscribing hexagon of the HC cell
r_p	radius of the damping particles
n_p	total number of damping particles
n_c	number of cell filled with damping particles
ζ	damping ratio
\mathbf{q}_i	generalized modal coordinates
$\boldsymbol{\chi}_s, \boldsymbol{\chi}_b$	slave and boundary degree freedoms
Φ_i	modal matrix
m_i, r_i	mass and radius of particle i
\mathbf{I}_i	mass moment of inertia of particle i
\mathbf{P}_i	position vector of the CM of particle i
\mathbf{g}	acceleration due to gravity
$\ddot{\Theta}$	angular acceleration of particle i
\mathbf{n}_{ij}	unit vector pointing from pointing from i to j
\mathbf{n}_{iw}	unit vector pointing from particle i to the center of contact point with wall w
$\mathbf{f}_{ij}, \mathbf{f}_{iw}$	force on particle i due to particle j or wall w
δ_{ij}, δ_{iw}	indentation
$\dot{\delta}_{ij}$	indentation velocity
k_n	Hertz constant
Ω	natural frequency matrix

m_{ij}^*	equivalent mass
α	Hertz damping constant
e_n	normal coefficient of restitution
μ	coefficient of Coulomb friction
ϕ_{mi}, ϕ_{ui}	measured and unmeasured coordinates of the i mode

1 Introduction

The sandwich laminates with aluminium face sheets and aluminium honeycomb (HC) core are the main structural members of a spacecraft equipment panel that host most of the subsystems. Though a honeycomb structure is lightweight making it suitable for the aerospace application, it has low damping resulting in high resonance responses. This may be potentially harmful for the mounted subsystems. Taking advantage of the porous HC structures, damping could be improved by inserting granules called damping particles (viscoelastic, aluminium, steel etc. material) in the empty cells (Wang and Yang, 2000; Michon et al., 2013; Koch et al., 2017; Panossian et al., 2004). These DPs dissipate the energy of a vibrating system in the form of heat, elastic wave and sound by collision among the particles and with cell walls. This technique requires no extra hardware or design modification, and it is simple and effective in wide frequency range and harsh environment. The impact damping technology has been used in vibration mitigation problem in civil structures (Lu et al., 2012), space shuttle and aerospace structures (Yao and Chen, 2013; Moore et al., 1995; Knight et al., 2013; Ahmad et al., 2016), oscillatory saws (Heckel et al., 2012) and automobiles (Duvigneau et al., 2016). Conventionally, DPs are filled in drilled holes (Xu et al., 2005; Xu et al., 2004) or a container filled with DPs are attached to the vibrating structures. The parameters involved in impact damping problem such as packing fraction, mass ratio, clearance, material and dimension of the DPs and enclosure, nature of vibration environment has been extensively studied (Vinayaravi et al., 2013; Masri and Caughey, 1966; Masri, 1970; Duncan et al., 2005; Gharib and Ghani, 2013). Very limited studies, mostly experimental, are available in literature on honeycomb treated with DPs. (Wang and Yang, 2000) carried out an experimental study on HC beams with solder balls as DPs. They reported a reduction of vibration response without damaging the cells and bonding. A similar study was conducted by (Michon et al., 2013) with hollow viscoelastic balls as DPs. They obtained the parameters of an equivalent viscous damper and used the equivalent model to predict the response of cantilever beam. They obtained the damping as a

function of the filling ratio and excitation frequency and reported significant improvement in the damping of the second mode of the beam.

A highly constrained system of DPs in the HC cells of the vibrating plate, where the particles and cell level interaction and its impact on the damping and the overall FRFs, have not been studied in detail. In this paper, the dynamics of DPs is modeled using discrete element method (DEM). The equations of motion of the cell walls are obtained by transferring the motion of the center of the cell, obtained from finite element model of the plate, to the walls assuming the planes defining the wall of the cells are rotating and translating as rigid planes. The forces, normal and tangential, involved in particle-wall contact is modeled by Hertz nonlinear dissipative model and Coulomb friction, respectively. A HC plate with edges under base excitation was considered for the numerical and experimental study. The FRFs obtained experimentally and numerically were compared. After validating the model, parametric study with respect to mass ratio and location of the filling area on the FRFs and damping is studied.

This paper is organized as follows: in section 2, we present the mathematical formulation of the discrete element method couple with plate dynamics. In the third section, the experimental setup and results are presented and compared with numerical predictions. Finally, in section 4, we present our conclusions.

2 Mathematical formulations

A honeycomb (HC) sandwich plate is made up of aluminium face sheets and HC core. The global coordinate system $\{XYZ\}$ with its origin at the geometric center of the plate and the local coordinate system $\{\bar{x}\bar{y}\bar{z}\}$ at the geometric center of a cell is shown in Figure 1.

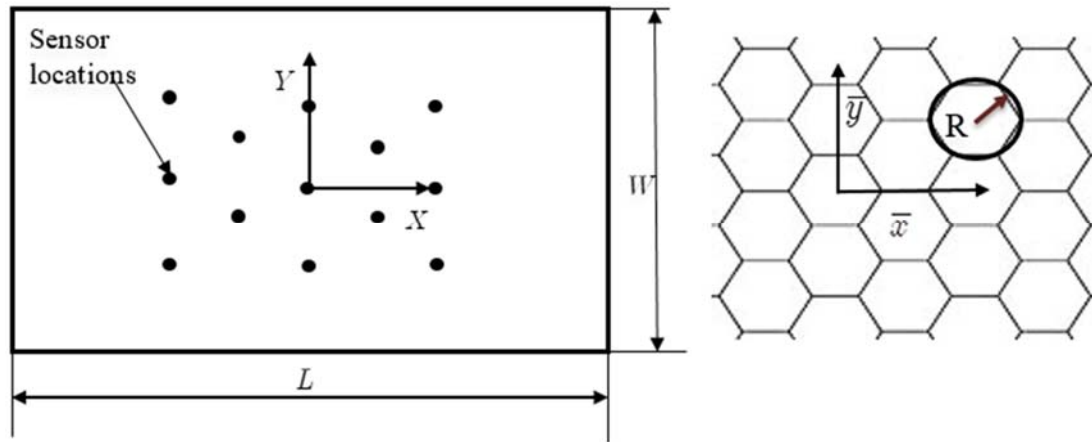


Figure 1. Honeycomb plate with coordinate systems

A finite element model of the HC plate is made in the ANSYS® software. The plate is discretized using a layered shell element 181 and the finite element mesh is shown in Figure 2a. The HC core is assumed orthotropic and the elastic constants of the core are obtained experimentally from the coupon level tests. Three tests, namely flatwise test, plate shear and three point bending tests are carried out on the coupon cut out from the same panel to estimate the mechanical properties. The test procedures and methods of estimation is described in reference (Kee Paik et al., 1999). The HC plate is meshed in such a way that some of the nodes are essentially placed exactly at the sensor locations so that the responses obtained from finite element analysis and from the experiments could be compared.

Special consideration in meshing is given to the areas of the HC where the core is filled with DPs. In this study, only the strategically chosen areas (Koch et al., 2017) of the plate are filled to minimize added mass (see Figure 2), and are chosen to be near the anti-node of the targeted mode where the displacement and velocities are maximum. The filled areas are seeded with nodes in such way that some of them are placed at the center of the cells and the displacements and the velocities of the nodes can be used to get the motion of the planes defining the walls of the cell. Furthermore, the motion of the walls of the neighboring cells are assumed to be similar as the formulation is for a plate having a dimension of a typical equipment panel used in spacecraft – the panel is much larger than the cell. Moreover, the damping forces arising from the impacts of the DPs in a cell can be assumed acting at the center-node of the cell. As the dimension of the cell is of few mm (compared to the plate, which is of the order of meter), same force can be assumed arising from the neighboring cells also and acting on the representative node. In Figure 2(b), the

neighboring cells and a representative node, node-19, where the sum of the damping forces arising from the neighboring cells is assumed acting, are shown. As a consequence, the impact damping force resulting from the immediate neighboring cells are assumed to be identical and hence the calculation of the dynamics of the DPs and the resulting forces for each honeycomb cell is not required. Here in this work, we propose to use a plate of size 1.4 m x 1.3 m (typical size of a spacecraft equipment panel) with damping patches of dimension 250 mm x 250 mm. Each such patch would contain around 2400 cells and each representative node is surrounded by six cells as shown in Figure 2.

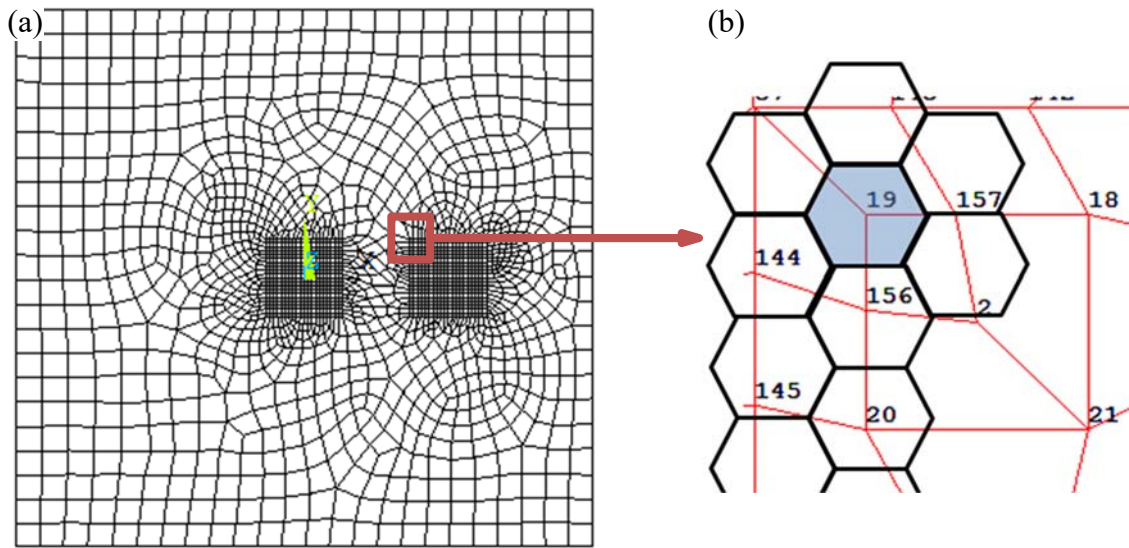


Figure 2. (a) Finite element mesh (b) Placement of node at the center of the cell

The governing finite element equations of HC plate are given as

$$\mathbf{M}\ddot{\boldsymbol{\chi}} + \mathbf{C}\dot{\boldsymbol{\chi}} + \mathbf{K}\boldsymbol{\chi} = \mathbf{f}^e + \mathbf{f}^d \quad (1)$$

The assembled displacement vector $\boldsymbol{\chi}$ consists of the nodal displacement vectors $[u \ v \ w \ \theta_x \ \theta_y \ \theta_z]^T$ where the displacements u and v are along the L -direction (X-axis) and W -direction (Y-axis) of the core, respectively, while w is along the out of plane normal direction. The angular rotations $[\theta_x \ \theta_y \ \theta_z]^T$ are defined as $[\partial u/\partial x \ \partial v/\partial y \ \partial w/\partial z]^T$. Equation (1) can be partitioned for base excitation problem as follows (Wijker, 2004)

$$\begin{bmatrix} \mathbf{M}_{ss} & \mathbf{M}_{sb} \\ \mathbf{M}_{bs} & \mathbf{M}_{bb} \end{bmatrix} \begin{Bmatrix} \ddot{\boldsymbol{\chi}}_s \\ \ddot{\boldsymbol{\chi}}_b \end{Bmatrix} + \begin{bmatrix} \mathbf{C}_{ss} & \mathbf{C}_{sb} \\ \mathbf{C}_{bs} & \mathbf{C}_{bb} \end{bmatrix} \begin{Bmatrix} \dot{\boldsymbol{\chi}}_s \\ \dot{\boldsymbol{\chi}}_b \end{Bmatrix} + \begin{bmatrix} \mathbf{K}_{ss} & \mathbf{K}_{sb} \\ \mathbf{K}_{bs} & \mathbf{K}_{bb} \end{bmatrix} \begin{Bmatrix} \boldsymbol{\chi}_s \\ \boldsymbol{\chi}_b \end{Bmatrix} = \begin{Bmatrix} \mathbf{f}_s^e \\ \mathbf{f}_b^e \end{Bmatrix} + \begin{Bmatrix} \mathbf{f}_s^d \\ \mathbf{f}_b^d \end{Bmatrix} \quad (2)$$

where the subscripts s and b denote the slave and boundary degree of freedoms (dofs), respectively, and the base acceleration is enforced on the χ_b dofs. The first part of the equation (2) is given as

$$\mathbf{M}_{ss}\ddot{\chi}_s + \mathbf{C}_{ss}\dot{\chi}_s + \mathbf{K}_{ss}\chi_s = \mathbf{f}_s^d + \mathbf{f}_s^e - (\mathbf{M}_{sb}\ddot{\chi}_b + \mathbf{C}_{sb}\dot{\chi}_b + \mathbf{K}_{sb}\chi_b) \quad (3)$$

The equation (3) can be written in the modal space using the transformation $\chi_i = \Phi_i \mathbf{q}_i$, where the modal matrix Φ_i is obtained from the eigenvalue problem: $(\mathbf{K}_{ii} + \Omega_{ik}^2 \mathbf{M}_{ii})\Phi_{ik} = 0$, invoking the orthogonality relation with respect to mass and stiffness matrix and assuming $\mathbf{C}_{ib}\dot{\chi}_b = \mathbf{0}$ as a consequence to diagonalizable viscous damping, as

$$\ddot{\mathbf{q}}_i + 2\zeta\Omega\dot{\mathbf{q}}_i + \Omega^2\mathbf{q} = \Phi_i^T(\mathbf{f}_i^d + \mathbf{f}_i^e) - \Phi_i^T(\mathbf{M}_{ib}\ddot{\chi}_b + \mathbf{K}_{ib}\chi_b) \quad (4)$$

In equation (4), the damping particle force \mathbf{f}_i^d is the only unknown. Evaluation of force vector \mathbf{f}_i^d resulting from the impact of damping particles against the walls of the honeycomb cell requires the knowledge of the motion of the particles as well as the walls of the honeycomb cell. The equations of motion of the particle i that is in contact with n_1 number of neighboring particles and n_2 points with cell walls can be written as

$$m_i\ddot{\mathbf{p}}_i = -m_i\mathbf{g} + \sum_{j=1}^{n_1} \mathbf{f}_{ij} + \sum_{w=1}^{n_2} \mathbf{f}_{iw} \quad (5)$$

$$\mathbf{I}\ddot{\boldsymbol{\theta}} = \sum_{j=1}^{n_1} \left(r_i - \frac{\delta_{ij}}{2}\right) \mathbf{n}_{ij} \times \mathbf{f}_{ij} + \sum_{w=1}^{n_2} (r_i - \delta_{iw}) \mathbf{n}_{iw} \times \mathbf{f}_{iw} \quad (6)$$

The indentations during impact, δ_{ij} and δ_{iw} , are illustrated in Figure 3.

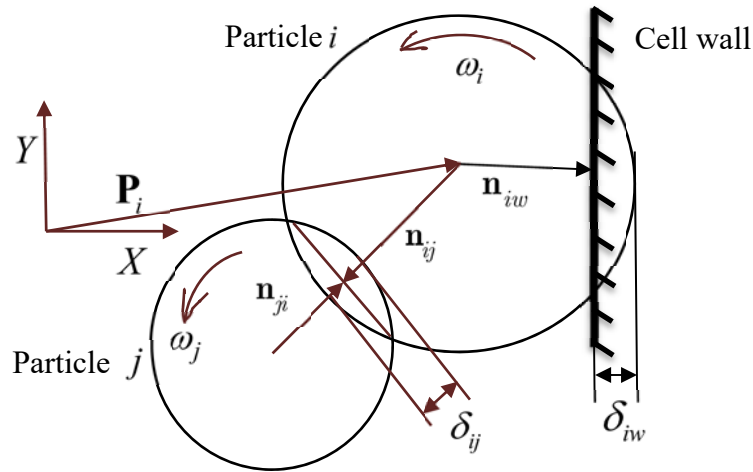


Figure 3. Parameters in a particle-particle and particle-cell wall impact phenomenon

Equations (5) and (6) involve the particle-wall contact force \mathbf{f}_{iw} which requires expressions for the position of cell walls where the damping particles are filled in. Let the geometric center of a cell of the honeycomb plate, at location $[x_i, y_i]$, undergoes deflection w and rotations $[\frac{dw}{dx}, \frac{dw}{dy}]$. Then the equation of planes defining the deformed walls, as shown in Figure 4, can be written as:

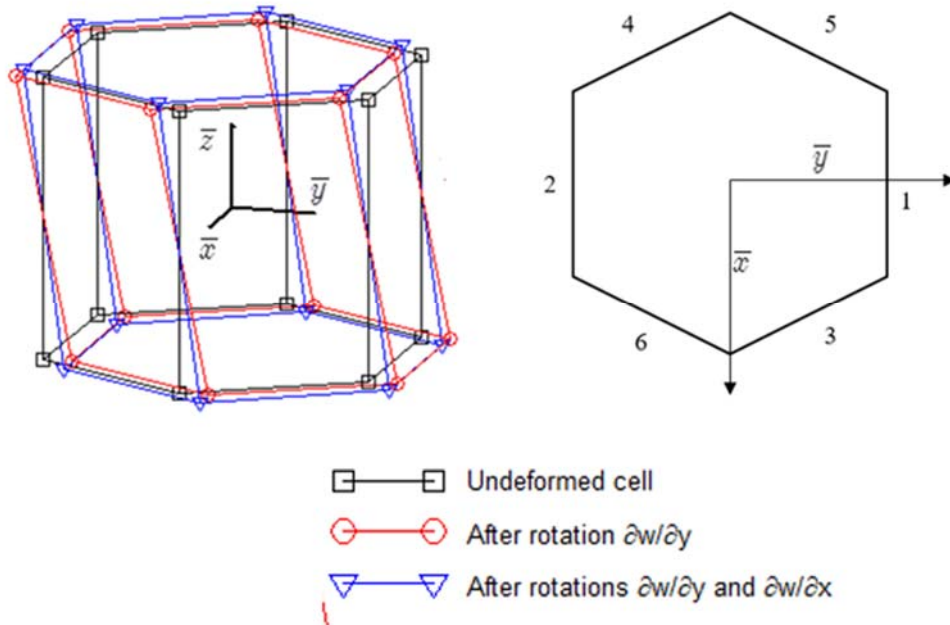


Figure 4. Deformation of the walls of a honeycomb cell.

Top and bottom planes

$$\bar{z} \pm \frac{t_c}{2} = 0 \quad (7)$$

Planes 1 and 2

$$\bar{y} + \frac{\partial w}{\partial y} \bar{z} \pm \frac{\sqrt{3}}{2} R = 0 \quad (8)$$

Planes 3 and 4

$$\bar{x} + \frac{\bar{y}}{\sqrt{3}} + \left(\frac{\partial w}{\partial x} + \frac{1}{\sqrt{3}} \frac{\partial w}{\partial y} \right) \bar{z} \pm R = 0 \quad (9)$$

Planes 5 and 6

$$\bar{x} - \frac{\bar{y}}{\sqrt{3}} + \left(\frac{\partial w}{\partial x} + \frac{1}{\sqrt{3}} \frac{\partial w}{\partial y} \right) \bar{z} \pm R = 0 \quad (10)$$

Equations (7) - (10) are with respect to a frame of reference attached to the geometric center of the cell. The cell walls undergo translation and rotations equal to the geometric center of the cell. From the knowledge of deflection and slope of the geometric point of the cell and position of the DP, the local indentation can be calculated by computing the distance from the center of the particles to cell walls (see the detailed mathematical procedure in (Ahmad et al., 2017)).

The impact forces are evaluated as follows: let there are n number of particles in the cell j that is at the location $[x_j, y_j]$ and a particle i is exerting a force \mathbf{f}_{iw}^d on the walls of the cell then the total force on cell walls due to n particles can be written as

$$\mathbf{f}_j^d = \sum_{i=1}^n \mathbf{f}_{iw}^d(x_j, y_j) \quad (11)$$

The force vector \mathbf{f}_i^d in equation (4) is obtained from the assemblage of nodal force vectors \mathbf{f}_j^d

The contact force between particle-particle or particle-wall consists of normal and tangential components is given as

$$\mathbf{f}_{ij} = \mathbf{f}_{ij}^n + \mathbf{f}_{ij}^t \quad (12)$$

Since low velocity impact is involved among the DP and particle – wall, an elastic dissipative nonlinear model for the normal component can be used. In this work, the model proposed by Tsuji et al. (Tsuji et al., 1992) and in vibrations problems by (Saeki, 2005; Fang et al., 2007) is used.

The expression for the normal component \mathbf{f}_{ij}^n is given by

$$\mathbf{f}_{ij}^n = - \left(k_n (\delta_{ij}^n)^2 + \alpha \sqrt{m_{ij}^* k_n} (\delta_{ij}^n)^{\frac{1}{4}} \dot{\delta}_{ij}^n \right) \mathbf{n}_{ij} \quad (13)$$

where δ_{ij}^n is the normal relative velocity of the center of particle i with respect to the center of particle j and the equivalent mass m_{ij}^* in equation (13) is defined as

$$m_{ij}^* = \frac{m_i m_j}{m_i + m_j} \quad (14)$$

α is the damping constant and a nonlinear function of the normal coefficient of restitution e_n (Tsuji et al., 1992), given as

$$\alpha = -\ln(e_n) \sqrt{\frac{5}{\ln(e_n)^2 + \pi^2}} \quad (15)$$

The elastic Hertz's constant k_n for spherical impacting bodies and sphere-plan wall is given in (Stronge, 2004). The simplest and most efficient approach to model the tangential contact force is to use the Coulomb's law of sliding friction (Johnson, 1985). Coulombs law has been used by many researchers in DEM for predicting vibration responses (Saeki, 2005; Saeki, 2002; Olson, 2003; Lu et al., 2010; Lu et al., 2012; Fang et al., 2007) and the Coulomb force is givens as

$$\mathbf{f}_{ij}^t = -\mu \left| \mathbf{f}_{ij}^n \right| \frac{\mathbf{V}_{ij}^t}{\left| \mathbf{V}_{ij}^t \right|} \quad (16)$$

The method for computing relative tangential component \mathbf{V}_{ij}^t can be found in (Ahmad et al., 2017). The equations of motion of the HC plate and DPs, equations (4) - (6), are solved simultaneously using Runge-Kutta method in MATLAB software. The DEM formulation described above assumes that the motion of any particle is affected by its immediate neighborhood contacts only. This require very small integration time step, at least one order less than the period of contact, and in this work, a time step 10^{-6} s is used. The local vibrations of the cell walls are ignored since the stiffness of local indentation is much higher than the bending stiffness of the cell wall. (Lu et al., 2010) reported that a frequency ratio of greater than 20 is appropriate to represent a stiff barrier whereby the compliance of the barrier can be ignored.

3 Experimental works and comparisons

3.1 Test setup and specimen

The HC plate with aluminium face sheets and core with geometric and material properties given in Table 1 was used in the experimental work. The plate is equipped with 13 accelerometers (make: Brüel & Kjær, Model: 4517-002, sensitivity approximately 10 mV/g) is shown in Figure 5(a).

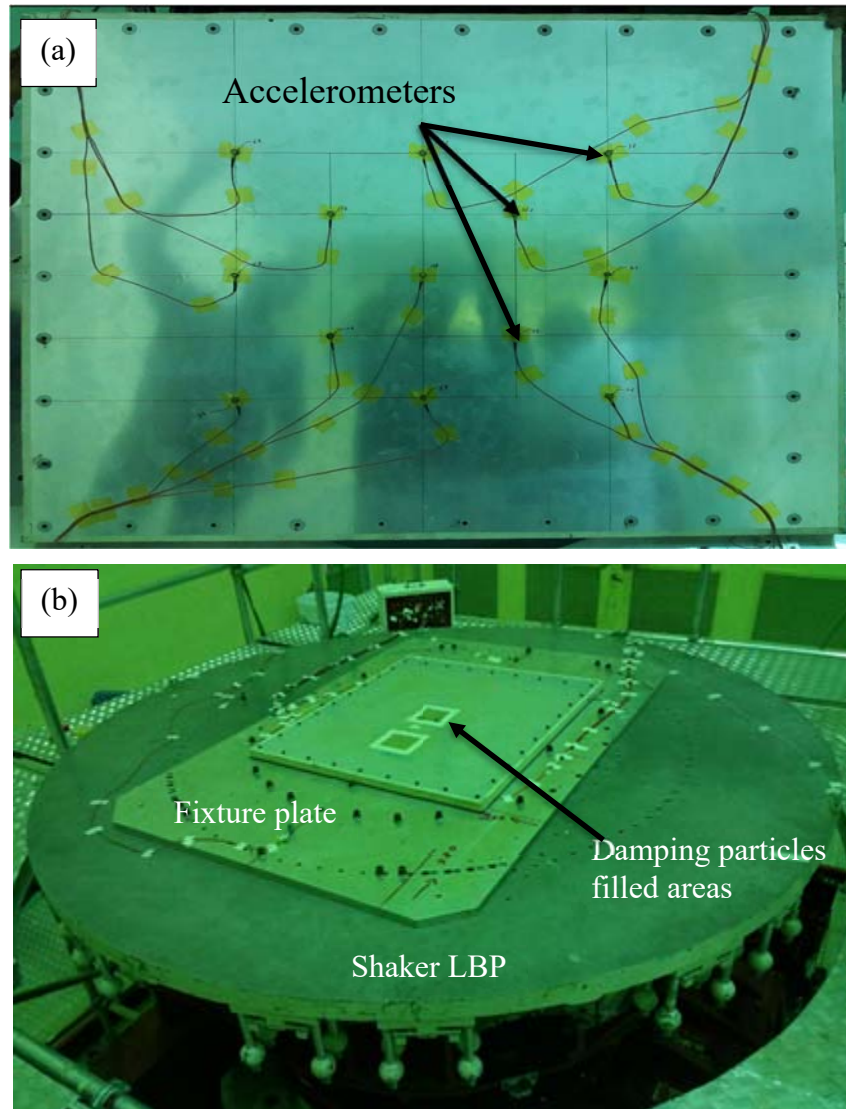


Figure 5. (a) Honeycomb sandwich plate, (b) The HC plate mounted on LBP of the electrodynamic shaker

The accelerometers are strategically placed to capture the lower modes of the plate. The edge of the honeycomb plate is fixed to a vibration fixture with M6 bolts passing through the especially design inserts embedded in the plate. The vibration fixture plate has a cutout in the central portion to allow the out-of-plane motion of the HC plate. The vibration fixture plate is mounted on the load bearing platform (LBP) of an electrodynamic shaker (LDS-V994, force rating 289.1 kN) as shown in Figure 5(b). A 250-channel data acquisition system (DAS) from Spectral Dynamics® was used for acquiring the acceleration data from the 13 accelerometers mounted on the backside of the plate as shown in Figure 5(a). Two patches of dimension 250 mm x 250 mm is marked on the HC plate using a paper tape. These are the areas where DPs are filled individually or together, depending on the modes to target. Acrylic damping particles are chosen for experimental study whose properties are given in Table 2(a) and 2(b). The metallic and heavy damping particle are ruled out because not only they add large amount of mass to system (resulting in significant change of the system itself) but they may also damage the cell walls of a honeycomb, which are made of 0.7 μ m thick aluminum foil. Another reason for choosing acrylic-damping particles is its temperature stability and lesser out gassing effect – the outgassing effect is crucial as materials tends to evaporate in extremely low-pressure environment of space. Each patch covers 2400 hundred cells of honeycomb core which when filled fully, 100%, contain 86400 damping particles. The mass of the damping particles under each patch is 427 grams, which is 10.7% of the 4.004 kg plate mass. The total mass of the DPs is to be limited to around 20% as the main purpose of using the HC plate in spacecraft and aerospace applications is to reduce the structural mass. Therefore, damping particles are added at discrete locations where modal displacement and velocities of targeted modes are maximum.

Table 1. Material and geometric properties of honeycomb plate

Properties	Units	Face-sheet (AA 2024 T3)	Honeycomb core (CR 3/16-5056-0.0007-P-32)
Length, L	mm	1400	1400
Width, W	mm	1300	1300
Thickness	mm	0.25	25.4
Density	kg/m ³	2800	32.1
Young's modulus	N/m ²	72×10^9	$E_{xx} = E_{yy} = E_{zz} = 10000$
Poisson's ratio		0.33	$\nu_{xy} = \nu_{yz} = \nu_{xz} = 0.3$
Shear modulus	N/m ²	-	$G_{xy} = 10000$ $G_{yz} = 0.89 \times 10^8$ $G_{xz} = 1.85 \times 10^8$
Diameter of inscribing circle of hexagonal cell	mm	-	4.76

Table 2(a). Properties of damping particles

Properties	Units	Aluminum	Acrylic
Radius	mm	-	1
Density	kg/m ³	2850	1180
Young's modulus	N/m ²	70×10^9	2.84×10^9
Poisson's ratio	-	0.33	0.402

Table 2(b) Properties of damping particles

Material pairs	-	Coefficient of sliding friction	Normal restitution coefficient
Acrylic – acrylic	-	0.096	0.70
Acrylic – aluminium	-	0.14	0.70

3.2 Modal survey test

A modal survey test was done on the HC plate without DPs to obtain the modal parameters such as damping ratio, natural frequencies and modal vectors. The edges of the plate were subjected to a linear sine sweep of constant amplitude with frequency sweeping from 10 Hz to 1000 Hz. Accelerometers mounted on the HC plate, see Figure 6, are located in such a way that they capture the lower modes of the plate.

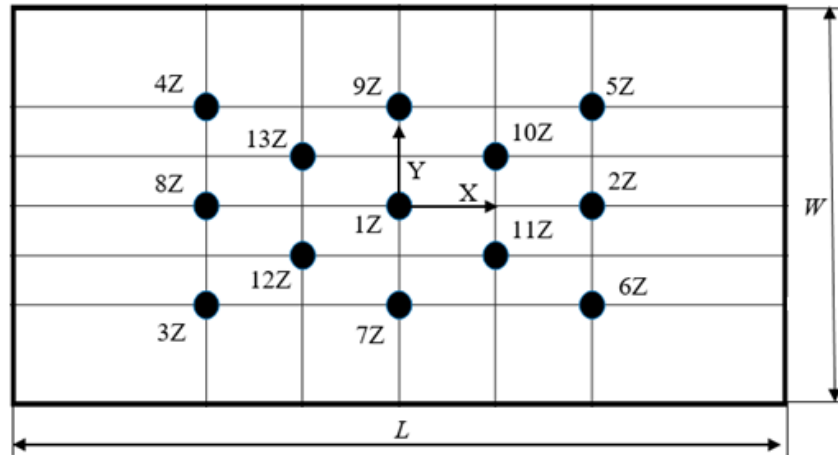


Figure 6. Accelerometers (1Z-13Z) on HC plate

The acceleration measurements were performed with a sampling rate of 12.8 kHz, well above the Nyquist criterion, as we are interested in frequencies up to 1000 Hz. The FRF estimation was carried out with the parameters as follows: resolution - 0.5 Hz; window – Hanning. The FRFs from the 13 accelerometers are given in Figure 7. The sensor 1Z, at the center of the HC plate, is seen responding significantly to all modes excited under the bandwidth of interest and has the highest response for all the excited modes. Figure 7 shows that only four modes within 1000 Hz are well excited. The frequencies and damping ratios of these modes are listed in Table 3.

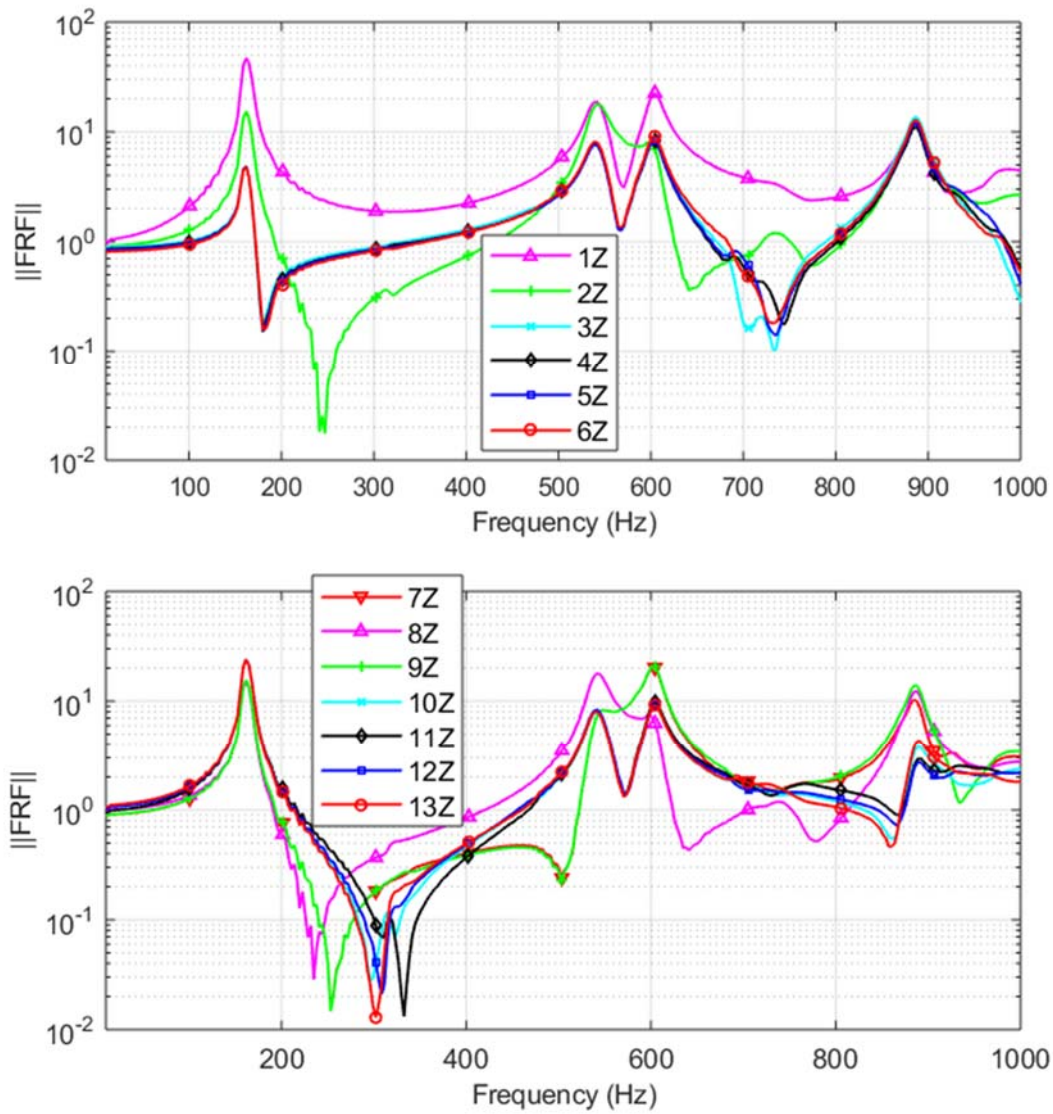


Figure 7. Experimental FRF of HC plate without DPs

Table 3. Frequencies and damping ratios of HC plate without DPs

Mode description	Frequency (Hz)	Damping ratio (experimental)
Mode-1	162.7	0.0227
Mode-2	541.4	0.0142
Mode-3	601.3	0.0158
Mode-4	884.5	0.0098

The measured mode shapes are obtained by expanding the measured dofs on the entire finite element domain by expansion using mass and stiffness matrix (EMS) method. In this method, the finite element mass and stiffness matrices are partitioned into measured ϕ_{mi} and unmeasured ϕ_{ui} dofs of mode i and using the measured natural frequency ω_i as (Friswell and Mottershead, 2013)

$$\left(-\omega_{mi}^2 \begin{bmatrix} \mathbf{M}_{mm} & \mathbf{M}_{mu} \\ \mathbf{M}_{um} & \mathbf{M}_{uu} \end{bmatrix} + \begin{bmatrix} \mathbf{K}_{mm} & \mathbf{K}_{mu} \\ \mathbf{K}_{um} & \mathbf{K}_{uu} \end{bmatrix} \right) \begin{Bmatrix} \phi_{mi} \\ \phi_{ui} \end{Bmatrix} = 0 \quad (17)$$

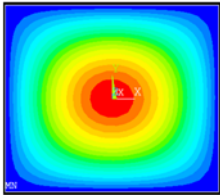
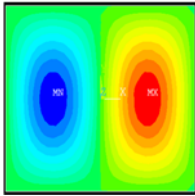
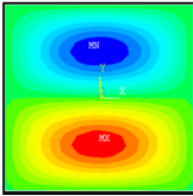
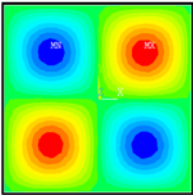
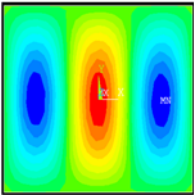
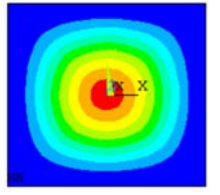
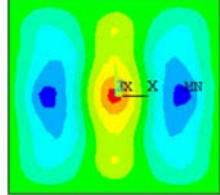
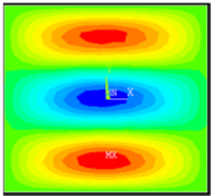
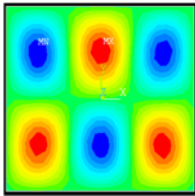
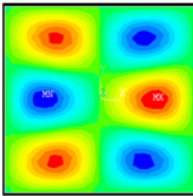
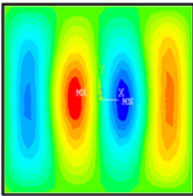
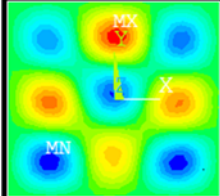
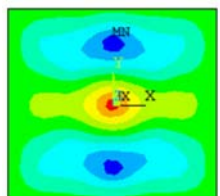
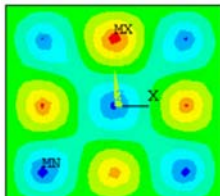
Equation (17) can be rearranged and solved for unmeasured coordinates as (Friswell and Mottershead, 2013):

$$\phi_{ui} = - \left[-\omega_{mi}^2 \mathbf{M}_{uu} + \mathbf{K}_{uu} \right]^{-1} \left[-\omega_{mi}^2 \mathbf{M}_{um} + \mathbf{K}_{um} \right] \phi_{mi} \quad (18)$$

The solution of equation (18) along with measured dofs form the complete modal vector that can be projected on ANSYS grid to get the experimental modes shapes. The mode shapes obtained experimentally by the method discussed above and from the normal mode analysis carried out in ANSYS software with all edges fixed is given in Table 4. The layered shell element, shell 181, was used from the ANSYS element library with free meshing and smart sizing 3 option. The Block Lanczos eigen value problem solver was chosen for modal analysis. Large numbers of modes of the plates are obtained in the modal analysis as given in Table 4, in comparisons to the modes, which were excited when HC plate was subjected to the same base excitation of all the four edges. An interesting observation is that only those modes of the plate where there is an anti-node at the center of the plate are excited. This is reflected in both experimental and computed FRFs. Many modes listed in Table 4, where there is no anti-node at the center of the plate, were not excited even though the resonance frequencies are well within the excitation bandwidth. It is easy to see that the mode at 316 Hz cannot be excited. One half of the plate moves in one direction, while the other part moves in the opposite direction at this mode. The excitation at the edge excites both areas in the same direction (in phase to the shaker).

As only thirteen accelerometers were mounted higher modes shapes cannot be uniquely established and correlated with FEM modes. The analytical damping matrix is constructed using the experimental damping ratios of the first four modes. However, for all other modes used in the mode superposition, it is assumed as 0.015.

Table 4. Mode shapes of the HC plate

FEM					
FEM	164.4 Hz	316.1 Hz	339.4 Hz	474.5 Hz	546.2 Hz
Test					
Test	162.7 Hz				541.4 Hz
FEM					
FEM	595.0 Hz	687.4 Hz	717.6 Hz	846.3 Hz	907.8 Hz
Test					
Test	601.3 Hz				884.5 Hz

3.3 Numerical simulations and validations

The experiments were carried out with DPs filled in an area of 250 mm x250 mm at the center of the plate with fill fractions 50%, 75% and 86.1%. The fill fraction is defined as the percentage of the volume of a cell filled with DPs. The different fill fractions are shown in Figure 8. The edges of the HC plate are excited with a constant acceleration (0.5 g) sine sweep of bandwidth 10 Hz – 1000 Hz. Figure 9 – Figure 111 present the computed and experimental FRFs at locations 1Z, 2Z, 5Z and 10Z for fill fractions of 50 %, 75% and 86.1%, respectively. The locations 1Z, 2Z, 5Z and 10 are chosen to estimate FRFs as these points lie at the points of maximum response of the targeted modes. The FRFs profiles are reasonably similar. However, the deviation in the higher frequency range is more, and there is a difference of 24 Hz in the fourth mode. The damping ratios of the four modes extracted from the FRFs are given in Table 5. Experimental results show that the damping ratios increase with fill fraction until it reaches a maximum in the fill fraction range of 75% to 86.1%. However, the computed damping ratios show the maxima at slightly higher fill fractions.

Table 5. The computed and experimental damping ratios with a single filling area at the center

Fill fraction	Mode – 1		Mode – 2		Mode – 3		Mode – 4	
	Exp.	Comp.	Exp	Comp	Exp	Comp	Exp	Comp
0%	0.0227	-	0.0142	-	0.0158	-	0.0098	-
50%	0.0301	0.0308	0.0230	0.0238	0.0183	0.0206	0.0149	0.0152
63.9%	-	0.0457	-	0.0252	-	0.0223	-	0.0165
75%	0.0426	0.0505	0.0241	0.0260	0.0212	0.0227	0.0178	0.0172
86.1%	0.0407	0.0552	0.0235	0.0263	0.0187	0.0230	0.0156	0.0176
94.4 %	-	0.0582	-	0.0261	-	0.0226	-	0.0178
100%	-	0.0558	-	0.0254	-	0.0235	-	0.0176

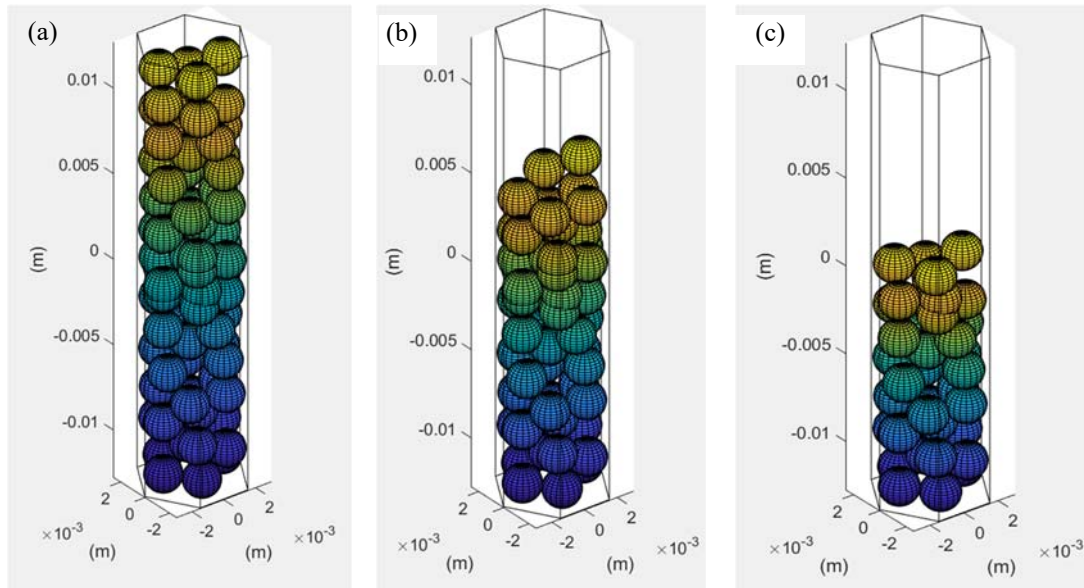


Figure 8. Honeycomb cells filled with damping particle (a) 100 % fill fraction, (b) 75% fill fraction and (c) 50% fill fraction

The error in damping ratios are large when fill fraction is more, it may be due to the fact that the as the fill fraction is increased the motion of the DPs are more of inter-granular and rubbing nature rather than impact as free space is getting more and more constrained. The friction is the dominant dissipation mode at higher fill fractions in the honeycomb system. The Coulombs law of friction, which has been used in developing the DEM model, does not take into account the tangential compliance and sticking phase of contact phenomenon, which dictates the post-contact dynamics and energy dissipation due to friction forces.

There is a large dip in the experimental FRFs at location 5Z shown in Figures 8,9 and 10 between 3rd and 4th mode. The dip in the FRF between the two resonance peaks is called anti-resonance, which is formed by superposition of negative region / roll-off region of first peak and positive region build up region of the next peak. The magnitude of dip depends on the damping of the peaks. A large dip is attributed to lower damping of the peaks. It can be seen in Table 6, the damping ratios of experimental FRFs for mode 3rd and 4th are smaller than that of the computed one except for the case of 75% where both are comparable. This is the reason why there is a smaller dip at anti-resonance as compared to 50% and 86.1%.

The change in the damping ratio for the lower two modes are insignificant with an increase in fill fraction after reaching the maxima. For other modes decreases is relatively sharp. One of the consequence of this study is that we do not have to fill the honeycomb structure beyond a certain

fill fraction. This can be intuitively explained by the fact that if the fill fraction is very large, there is very little momentum exchange and the damping increases only due to Coulomb friction.

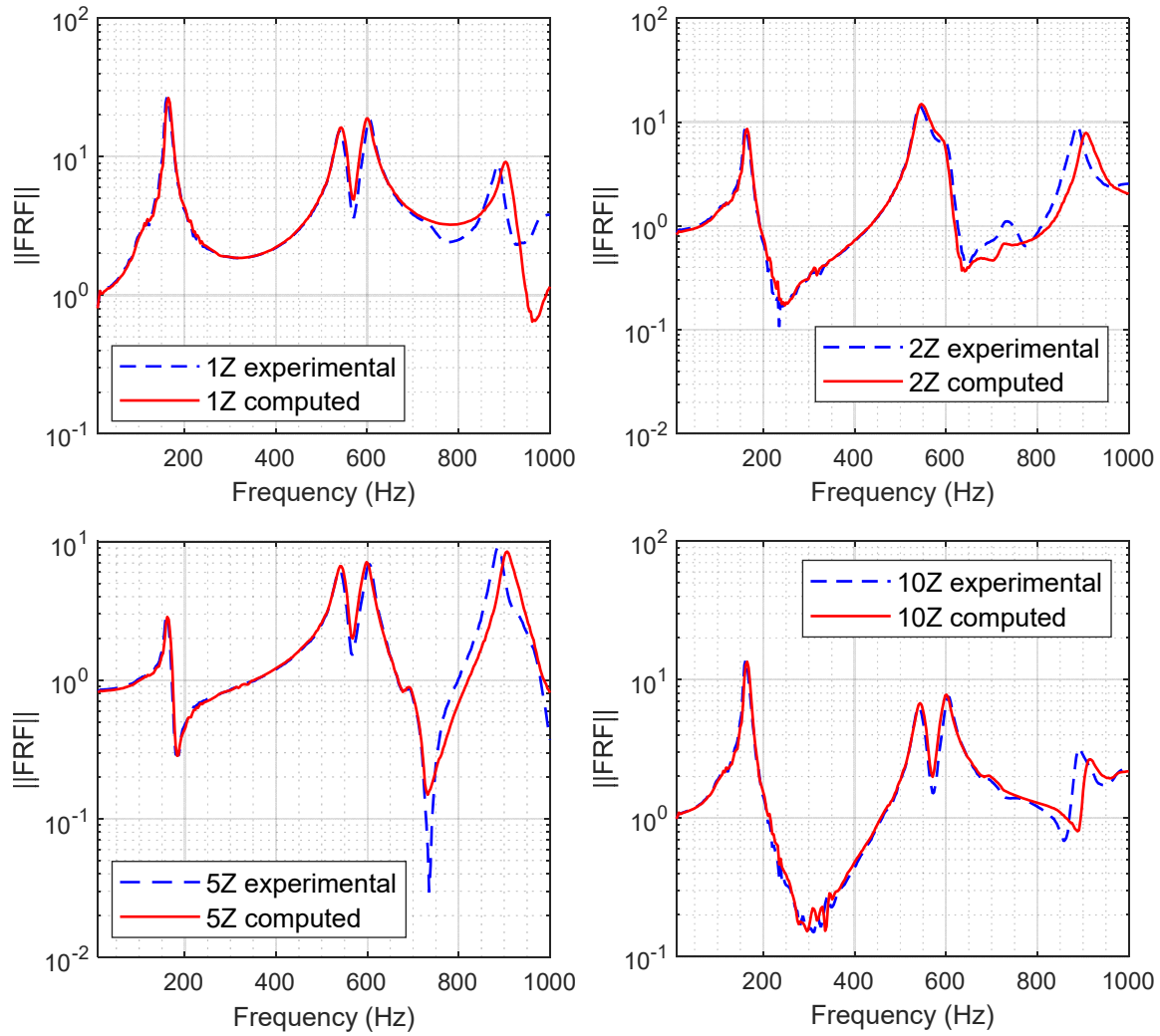


Figure 9. Experimental and computed FRFs for 50 percent fill fraction.

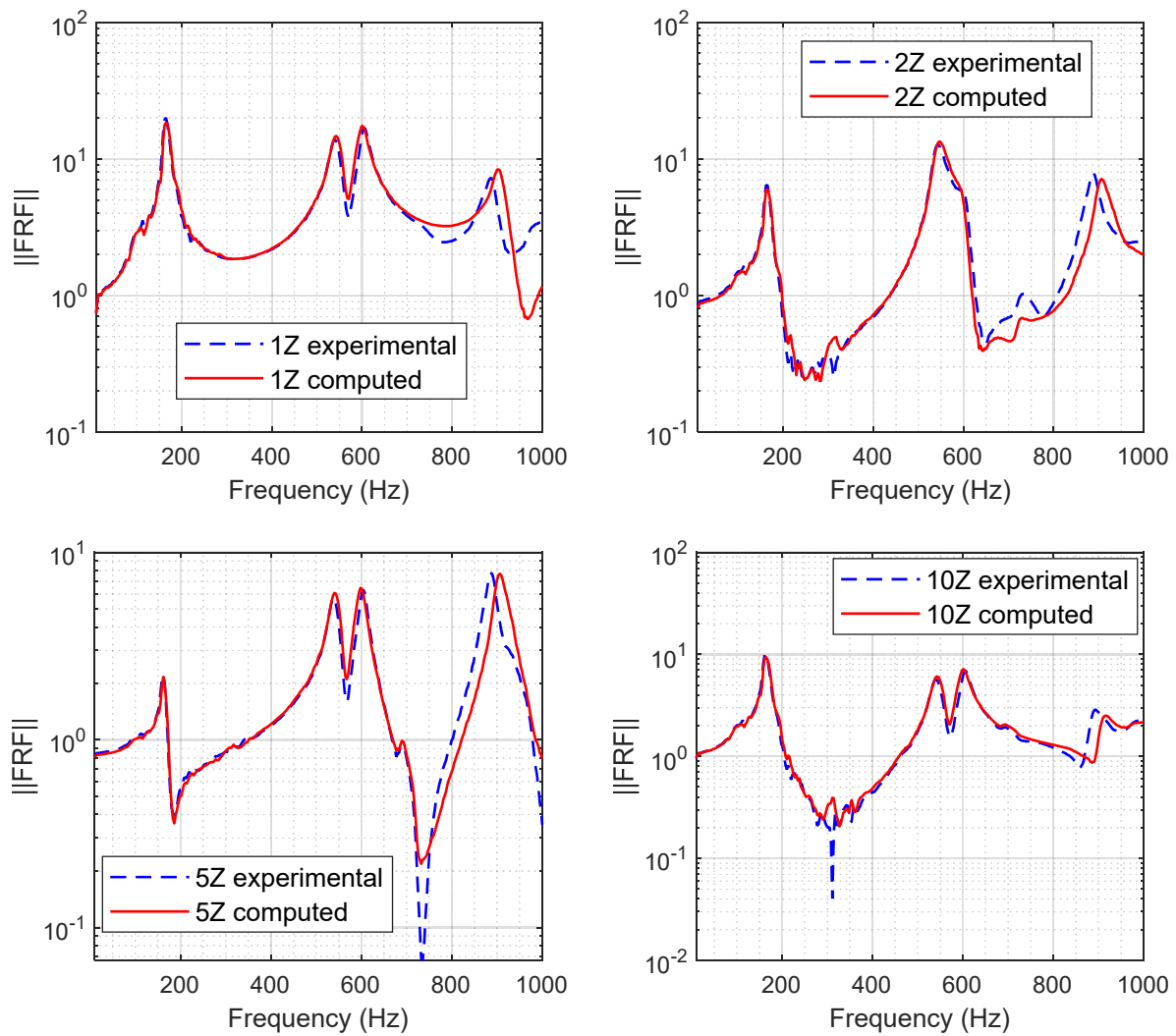


Figure 10 Experimental and computed FRFs for 75% percent fill fraction.

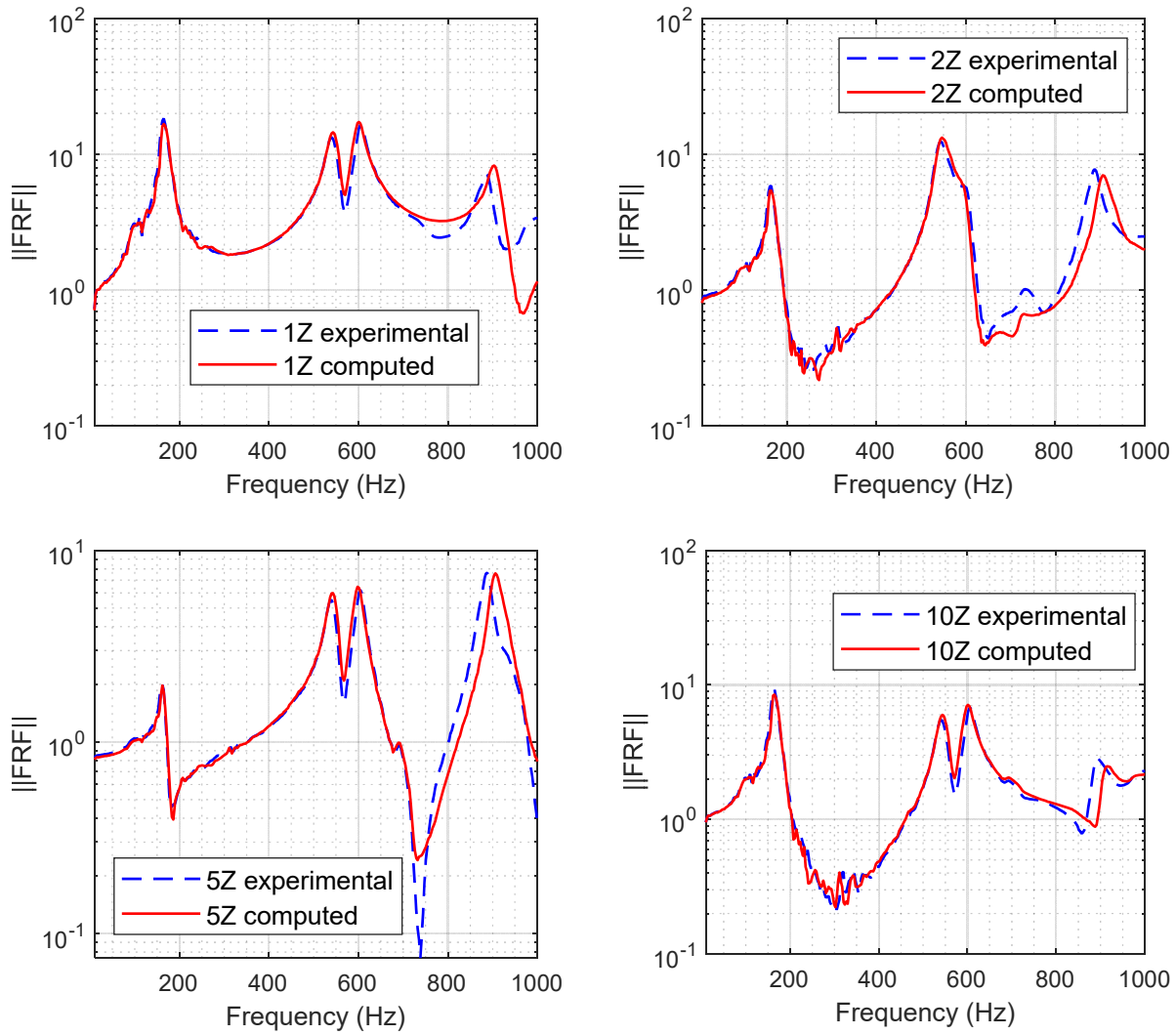


Figure 11. Experimental and computed FRFs for 86.1% percent fill fraction.

Table 6 gives the damping ratio when the damping particles are filled at two places covering an area of 250 mm x 250 mm each. The filled areas are at the center and at location $(L/3, 0)$ of the plate. Two tests were conducted with the same sine sweep edge acceleration and for the fill fractions 75% and 86.1%. Though the mass of the DPs has increased two times, the change in the damping for the mode-2 to mode-4 is less than 15%. An improvement of 19% and 39.1% in the damping ratios of the first mode are observed for 75% and 86.1% fill fractions. The FRFs at locations 1Z and 2Z are compared with the single area filled with DPs in Figure 12 and Figure 13. The FRFs are similar to the case of the single area filled with the reduced first mode.

Table 6 : Damping ratios when two areas are filled with DPs

Fill fraction	Mode – 1	Mode – 2	Mode – 3	Mode – 4
75%	0.0511	0.0261	0.0206	0.0187
86.1%	0.0566	0.0265	0.0211	0.0199

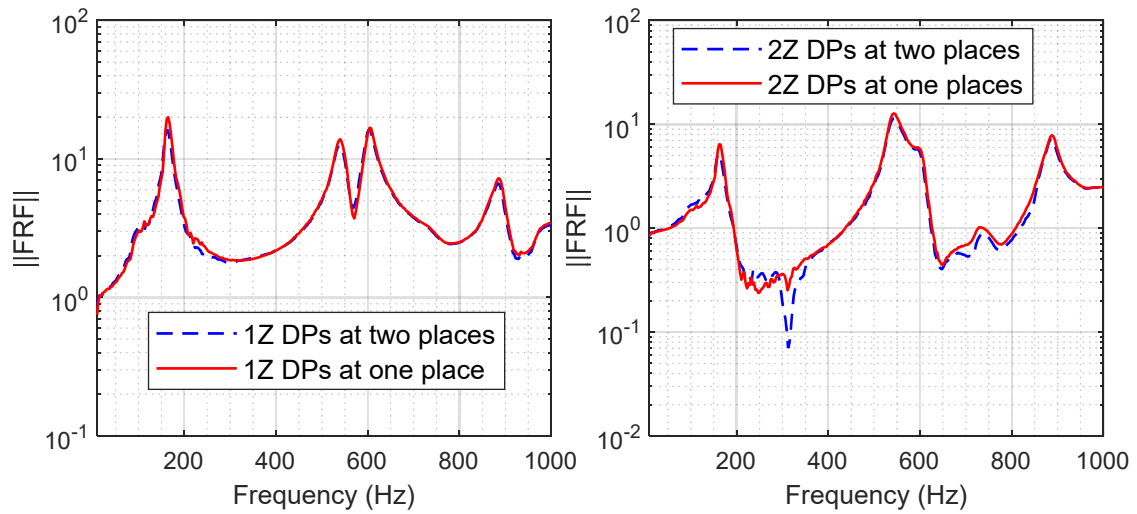


Figure 12. FRF with 75% fill fraction, DPs at two places

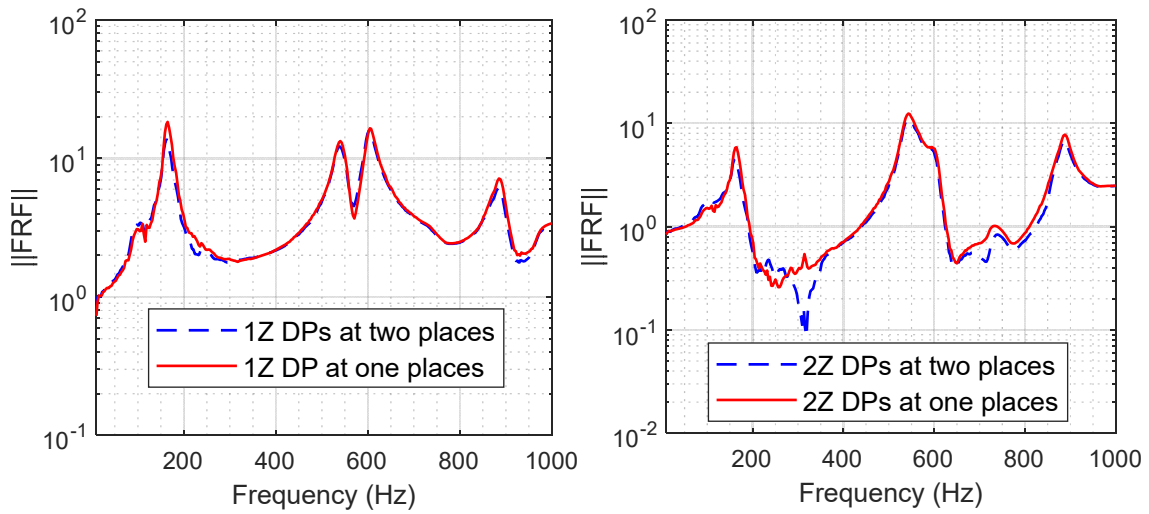


Figure 13. FRF with 86.1% fill fraction DPs, at two places

4 Conclusions

The vibration attenuation behavior of a honeycomb (HC) plate treated with damping particles is studied experimentally and numerically. A mathematical model using discrete element modeling captures the coupled dynamics of damping particles (DPs), motion of cell walls of the honeycomb core and motion of plate. An HC plate partially filled with DPs and excited at all the four edges with constant amplitude sine sweep signal was studied. The coupled equations of motion of damping particles and HC plate were solved using numerical method to obtain the damping ratios, resonance peaks and FRFs and these are compared with the experimental results. Four modes were captured up to 1000 Hz with an error of less than 5% in frequency between the computed and experimental values. The damping ratios obtained from computations and experiments are found to be matching well for lower fill fractions. However, for higher fill fractions the error is increasing. The error in computed values for resonance peaks is higher in larger fill fractions as a consequence of the error in damping ratios. The discrete element method (DEM) combined with finite element method (FEM) captures the complex coupled dynamics of damping particles and HC sandwich structures reasonably well. The correlation between and experimental and DEM-FEM model in terms of damping ratio and FRFs computed at different points on the plate is reasonably good. The DEM-FEM model for the system of damping particles and hexagonal honeycomb cell used the large number of parameters related to material and damping particle and the HC plate. The future work will be aimed towards determination of parameters of damping particle most effective in reducing the peak at resonance, determination of most effective location on the host structures for filling the damping particles and size of the area to be used for filling the damping particles. The model developed in this work can also be used for arriving at damping law for limited choice of parameters.

5 Acknowledgments

The authors would like to thank Mr. S Shankar Narayan, head, experimental structural dynamics division and engineers, Mr. Paandu Thalla and Mr. Sujeet Kumar, at Environmental Test Lab Facility, ISRO Satellite Centre, for their support in carrying out the experimental work. This research work is partially funded by ISRO-IISc Space Technology Cell (ISTC/MME/AG/394).

References

- Ahmad N, Ranganath R and Ghosal A. (2016) Assessment of particle damping device for large laminated structures under acoustic excitations. *Proceedings of 14th ISAMPE National Conference on Composites (INCCOM-14)*. Hyderabad.
- Ahmad N, Ranganath R and Ghosal A. (2017) Modeling and experimental study of a honeycomb beam filled with damping particles. *Journal of Sound and Vibration* 391: 20-34.
- Duncan MR, Wassgren CR and Krousgrill CM. (2005) The damping performance of a single particle impact damper. *Journal of Sound and Vibration* 286: 123-144.
- Duvigneau F, Koch S, Woschke E, et al. (2016) An effective vibration reduction concept for automotive applications based on granular-filled cavities. *Journal of Vibration and Control* 24: 73-82.
- Fang X, Tang J and Luo H. (2007) Granular damping analysis using an improved discrete element approach. *Journal of Sound and Vibration* 308: 112-131.
- Friswell M and Mottershead JE. (2013) *Finite Element Model Updating in Structural Dynamics*: Springer Netherlands.
- Gharib M and Ghani S. (2013) Free vibration analysis of linear particle chain impact damper. *Journal of Sound and Vibration* 332: 6254-6264.

- Heckel M, Sack A, Kollmer JE, et al. (2012) Granular dampers for the reduction of vibrations of an oscillatory saw. *Physica A: Statistical Mechanics and its Applications* 391: 4442-4447.
- Johnson KL. (1985) *Contact Mechanics*: Cambridge University Press.
- Kee Paik J, Thayamballi AK and Sung Kim G. (1999) The strength characteristics of aluminum honeycomb sandwich panels. *Thin-Walled Structures* 35: 205-231.
- Knight B, Parsons D, Smith A, et al. (2013) Evaluating Attenuation of Vibration Response using Particle Impact Damping for a Range of Equipment Assemblies. *AIAA Aerospace Design and Structures Event; 8-11 Apr. 2013*. Boston, MA; United States.
- Koch S, Duvigneau F, Orszulik R, et al. (2017) Partial filling of a honeycomb structure by granular materials for vibration and noise reduction. *Journal of Sound and Vibration* 393: 30-40.
- Lu Z, Lu X, Lu W, et al. (2012) Experimental studies of the effects of buffered particle dampers attached to a multi-degree-of-freedom system under dynamic loads. *Journal of Sound and Vibration* 331: 2007-2022.
- Lu Z, Lu X and Masri SF. (2010) Studies of the performance of particle dampers under dynamic loads. *Journal of Sound and Vibration* 329: 5415-5433.
- Masri SF. (1970) General Motion of Impact Dampers. *The Journal of the Acoustical Society of America* 47: 229.
- Masri SF and Caughey TK. (1966) On the Stability of the Impact Damper. *Journal of Applied Mechanics* 33: 586.
- Michon G, Almajid A and Aridon G. (2013) Soft hollow particle damping identification in honeycomb structures. *Journal of Sound and Vibration* 332: 536-544.

- Moore JJ, Palazzolo AB, Gadangi R, et al. (1995) A Forced Response Analysis and Application of Impact Dampers to Rotordynamic Vibration Suppression in a Cryogenic Environment. *Journal of Vibration and Acoustics* 117: 300.
- Olson SE. (2003) An analytical particle damping model. *Journal of Sound and Vibration* 264: 1155-1166.
- Panossian H, Kovac B and Rackl R. (2004) Composite Honeycomb Treatment via Non-Obstructive Particle Damping (NOPD). *45th AIAA/ASME/ASCE/AHS/ASC Structures, Structural Dynamics & Materials Conference, AIAA 2004-1689*. Palm Springs, California.
- Saeki M. (2002) Impact Damping with Granular Materials in a Horizontally Vibrating System. *Journal of Sound and Vibration* 251: 153-161.
- Saeki M. (2005) Analytical study of multi-particle damping. *Journal of Sound and Vibration* 281: 1133-1144.
- Stronge WJ. (2004) *Impact Mechanics*: Cambridge University Press.
- Tsuji Y, Tanaka T and Ishida T. (1992) Lagrangian numerical simulation of plug flow of cohesionless particles in a horizontal pipe. *Powder Technology* 71: 239-250.
- Vinayaravi R, Kumaresan D, Jayaraj K, et al. (2013) Experimental investigation and theoretical modelling of an impact damper. *Journal of Sound and Vibration* 332: 1324-1334.
- Wang B and Yang M. (2000) Damping of honeycomb sandwich beams. *Journal of Materials Processing Technology* 105: 67-72.
- Wijker J. (2004) *Mechanical vibrations in spacecraft design*, New York: Springer-Verlag Berlin Heidelberg.
- Xu Z, Wang MY and Chen T. (2004) An Experimental Study of Particle Damping for Beams and Plates. *Journal of Vibration and Acoustics* 126: 141.

Xu Z, Wang MY and Chen T. (2005) Particle damping for passive vibration suppression: numerical modelling and experimental investigation. *Journal of Sound and Vibration* 279: 1097-1120.

Yao B and Chen Q. (2013) Investigation on zero-gravity behavior of particle dampers. *Journal of Vibration and Control* 21: 124-133.